

Journal of Materials Chemistry A

Accepted Manuscript



This is an *Accepted Manuscript*, which has been through the Royal Society of Chemistry peer review process and has been accepted for publication.

Accepted Manuscripts are published online shortly after acceptance, before technical editing, formatting and proof reading. Using this free service, authors can make their results available to the community, in citable form, before we publish the edited article. We will replace this *Accepted Manuscript* with the edited and formatted *Advance Article* as soon as it is available.

You can find more information about *Accepted Manuscripts* in the [Information for Authors](#).

Please note that technical editing may introduce minor changes to the text and/or graphics, which may alter content. The journal's standard [Terms & Conditions](#) and the [Ethical guidelines](#) still apply. In no event shall the Royal Society of Chemistry be held responsible for any errors or omissions in this *Accepted Manuscript* or any consequences arising from the use of any information it contains.

Cite this: DOI: 10.1039/c0xx00000x

Full Paper

www.rsc.org/xxxxxx

Observation of lithiation induced structural variations in TiO₂ nanotube arrays by X-ray absorption fine structures

Dongniu Wang,^{a,b,d} Lijia Liu,^c Xueliang Sun^{a*} and Tsun-Kong Sham^{b*}

Received (in XXX, XXX) Xth XXXXXXXXX 20XX, Accepted Xth XXXXXXXXX 20XX

DOI: 10.1039/b000000x

We report herein a study of self-organized TiO₂ nanotube arrays both in amorphous and anatase phase with superior electrochemical performance upon lithiation and delithiation. The X-ray absorption fine structure study at the Ti K-, L-, O K- and Li K-edges have been conducted to track the behavior. Characteristic features for amorphous and anatase TiO₂ are identified. After lithiation, it is found that although no obvious chemical states variation is apparent at the Ti K and L edge, charge transfer from Ti 3d to O 2p and also partially amorphization of anatase TiO₂ are evident from spectral intensities. The Li and O K edge XAFS show the successful intercalation of lithium and reveal the existence of a nearly linear “O-Li-O” arrangement in lithiated TiO₂ nanotube. This study helps understanding lithiation process in nanostructured TiO₂ anodes from spectroscopic view.

Introduction

Nanostructured TiO₂ has been extensively studied and used in photodegradation devices,¹ energy harvesting systems such as dye-sensitized photovoltaic cells^{2,3}, energy storage systems such as electrochemical capacitors⁴ and lithium ion batteries.⁵⁻⁸ Especially, TiO₂ intrigues great interests in battery fields due to its high working potential and superior stabilities, where efforts are being made to expand applications in heavy duty systems such as electrical and hybrid electrical vehicles. In order to attain cells with both high energy density and power densities, great attention has been focused on exploring various TiO₂ nanostructures with different phases.⁹⁻¹² Further, the geometry or configuration could also significantly affect the performances of TiO₂. Fang¹³ et al. and Han¹⁴ et al. demonstrate that the one dimensional self-assembled arrays still exhibit excellent electrochemical behaviors at high current and power densities up to 30 A g⁻¹ and 10 C, respectively, which is ascribed to the reduced resistance between electrode and current collectors and also the improved efficiency for electrons transportation along one dimensional channels.¹³⁻¹⁷ Despite the superior electrochemical performances, gleaning a comprehensive understanding of the effect of intercalated lithium ions into TiO₂ framework upon alternations of their structures and chemical states is of paramount significance on both the understanding of the mechanism and the optimization of the engineering design. Since the report by Whittingham et al.,¹⁸ the insertion of lithium into a TiO₂ framework has been intensively studied in which lithiation was conducted both chemically using *n*-butyllithium and electrochemically.^{7, 19-23} Among various characterization techniques such as Raman, NMR,²¹ and XRD,²⁴ X-ray absorption

fine structure (XAFS) is arguably, the most powerful tool on illustrating the local structural evolution of element of interest upon lithiation. XAFS probes the modulation of core-level transitions (absorption coefficient) of an element of interest by its chemical environment in both the near edge and extended regions of the absorption coefficient above the threshold – commonly known as the X-ray absorption near-edge structure (XANES) and the extended X-ray absorption fine structure (EXAFS), respectively. XANES is an element, local structure and bonding specific method following the dipole selection rules. EXAFS arises from the interference of the outgoing and backscattering photoelectron wave at the absorbing atom and yields the information about local structure of atoms such as the interatomic distance between the absorbing atom and its neighboring atoms (bond length), coordination number, and Debye-Waller factor (mean square deviation of the bond length) in the first several shells.²⁵⁻²⁹

With regard to the structure of lithiated phases of TiO₂ (Li_xTiO₂, 0 < x < 1), extensive work has been conducted; for example, pioneering work from Ohzuku³⁰ claimed the cubic LiTiO₂ phase while Bonino²⁴ and Cava³¹ claimed the orthorhombic Li_{0.5}TiO₂ phase. Lafont et al.²³ performed an in-situ study and found that anatase TiO₂ undergoes a two-stage transition - An *Imma* orthorhombic Li_xTiO₂ is first formed at partially lithiated state followed by a cubic LiTiO₂ phase (*I4₁/amd*) in the fully lithiated state. More importantly, it should be noted that the stability and structure of Li_xTiO₂ are highly dependent on the pristine TiO₂ crystal phase (e.g. TiO₂-B,³² ramsdellite^{33, 34} and anatase³⁵) and corresponding morphology (e.g. nanoparticle^{19, 23} and nanotubes³⁶) of the TiO₂. Borghlos et al.³⁷ conducted the Ti K-edge XAFS study on the lithiated amorphous TiO₂ nanoparticles,

where a pre-edge shift toward lower energy and a new shoulder are found after lithiation which are attributed to the oxygen vacancies. Similarly, Okumura et al.³² also reported the t_{2g} peak shifted to the lower energy in the Ti L_{3} edge XANES spectra for submicrosized TiO_2 -B. XAS study of $Li_{2+x}Ti_3O_7$ ramsdellite³⁸ reveals that though host lattice remains unchanged upon lithiation, the Ti K-edge EXAFS analysis reveals a slight interatomic distances alternations and a reducing number of unoccupied O 2p densities of states in the O K-edge XANES. Since nanostructured anodes^{7, 11, 12, 21, 39, 40} exhibit improvement of the practical capacity approaching theoretical values and also high rate properties, it is crucial to gain additional insights to facilitate both fundamental and practical studies.

In this paper, we set up a protocol for high lithium ion battery (LIB) performance tracked by XAFS. We first synthesized the self-organized TiO_2 nanotubes arrays both in amorphous and anatase phases on Ti foil using an electrochemical anodization method and then conducted the lithiation with the electrochemical behaviors evaluated. Finally, a detailed XAFS analysis was conducted to investigate the effect of lithium intercalation on the structure of TiO_2 from the Ti, O and Li perspective.

Experimental Methods

Synthesis of TiO_2 NT: TiO_2 NT arrays were synthesized using a one-step anodization process by applying a DC (direct current) power supply with a voltage around 16V. Ti foil (0.1 mm thick, Goodfellow Ltd.) and a Pt wire are used as anode and cathode, respectively. A glycerol-based electrolyte was used in which HF (0.5 wt%) and glycerol are mixed in a volumetric ratio of 1:9. To facilitate the growth of nanotubes with smooth walls, a small amount of H_2O (~250 μ L) was added to the final mixture. Detailed procedures can be found in previously reported results.⁴¹ After 6 hours, the self-organized TiO_2 nanotube was formed aligning vertically onto the Ti foil substrate. Then the nanotubes were washed several times with deionized water and dried under a N_2 flow. In order to obtain a pure anatase phase,⁴¹ the as-prepared TiO_2 nanotubes were annealed at 550 $^{\circ}C$ for 2h, at which TiO_2 was fully crystallized into anatase.

Characterization: Samples were characterized by X-ray diffraction (XRD, Rigaku RU-200BVH with a Co-K α source ($\lambda=1.7892$ \AA)), field-emission scanning electron spectrometry (FE-SEM, Hitachi 4800S), and energy dispersive spectroscopy (EDS). The XAFS experiments were performed at the Canadian Light Source (CLS) located at the University of Saskatchewan. The Ti $L_{3,2}$ - and O K-edge XANES were measured at the undulator based Spherical Grating Monochromator (SGM) beamline;^{42, 43} the Ti K-edge EXAFS were obtained at the Soft X-ray Microcharacterization Beamline (SXRMB),⁴⁴ and the Li K-edges were conducted at the variable line spacing plane grating monochromator (VLS PGM) beamline.⁴⁵ Spectra were normalized to the incident photon flux, which was recorded using a refreshed Au mesh or a Ni mesh.

Electrochemical Measurement: The measurements were conducted using two-electrode cells. The as-obtained samples were cut into disks and dried at 80 $^{\circ}C$ under vacuum overnight to remove the adsorbed water and then directly used as the working electrode considering the good electronic conductivity of the Ti foil. Coin cells (CR2032 type) were assembled using lithium

metal foil as the counter electrode and the polypropylene as the separator inside an argon-filled glove box. The electrolyte was 1M $LiPF_6$ in ethylene carbonate /dimethyl carbonate solvent (EC/DMC, 1:1 in volume). The profiles of galvanostatically charging and discharging curves were obtained on a computer-controlled battery tester system (Arbin BT-2000) at a voltage range of 1 V to 3 V (vs. Li^+/Li) with a current density of 100 mA g^{-1} . The specific capacity is calculated based on the mass of TiO_2 NT, which was obtained by stripping the TiO_2 NT from the substrate using adhesive tape. The lithiated TiO_2 nanotubes samples were prepared by discharging the half cells to 1 V at 100 mA g^{-1} in the first cycle, and then were disassembled from the cell and washed thoroughly with ethanol and DMC.

Results and Discussion

The phase composition and crystallinity of the prepared TiO_2 NT arrays are identified by XRD, as shown in Figure 1a. The as-made TiO_2 NT is amorphous, exhibiting no peaks related to crystalline TiO_2 . The three peaks that can be observed come from the Ti foil substrate. The zoomed-in spectrum displays one broad peak centered at 30 $^{\circ}$, demonstrating its amorphous feature. EDS spectrum (Figure S1) for amorphous TiO_2 clearly shows the Ti and O characteristic fluorescence lines, further indicating the successful preparation of TiO_2 . After annealing, typical peaks for tetragonal anatase TiO_2 can be identified at (101), (004) and (200) planes (JCPDS No. 2-387), indicating a phase transformation to crystalline anatase TiO_2 had taken place. The typical anatase TiO_2 cell are shown in Figure 1b.

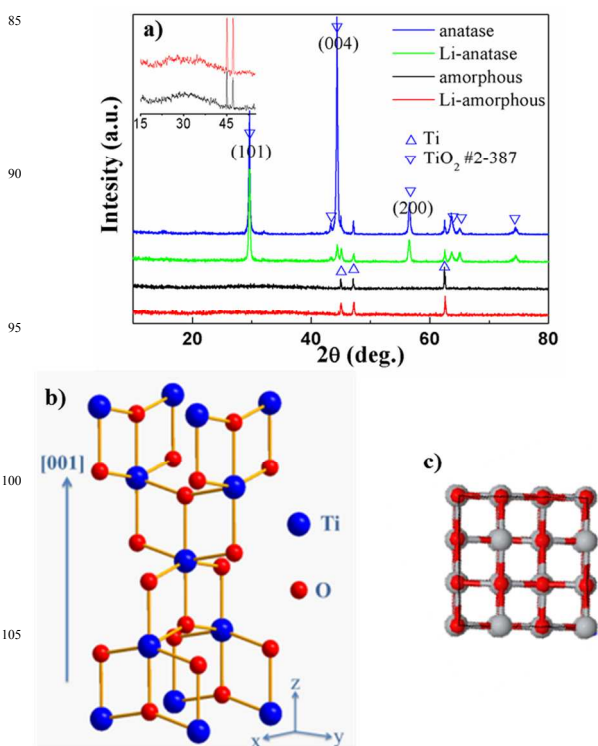


Figure 1. (a) XRD spectra of the amorphous and anatase TiO_2 NT before and after lithiation, inset is the magnified spectra with an angle between 15 and 45 degree. (b) Scheme of the TiO_2 anatase unit cell. (c) Top view showing the channels along [001] (Grey ball: Ti, Red ball: O).

The channels along the [001] direction are clearly observable from the top view in Figure 1c. Intriguingly, for both amorphous and anatase TiO₂ after electrochemical lithiation, no lithium-related new phase can be identified from the XRD spectra, and the original phase are well maintained, indicating that the lithiation process does not change the phase composition markedly. For anatase TiO₂, the (004) plane before lithiation exhibits usually high intensity compared to other planes, illustrating that the well crystallographically oriented TiO₂ NT arrays are along the [001] direction.⁴⁶ It is noted, however, that the intensity of the (004) diffraction decreases drastically after lithiation, indicating a distortion of the TiO₂ plane after the introduction of lithium, which preferentially interacts with TiO₂ along the [001] direction and locate in between (004) planes. It has been reported that the (004) plane has higher surface energy compared to other planes (e.g. (101) plane) which may facilitate the integration with lithium ions.⁴⁷ Since the lithiation process of TiO₂-based anodes is intercalation in nature, the introduction of lithium into TiO₂ does not significantly alter the integrity of the framework, as shown from the similar intensities and widths of other peaks of the lithiated TiO₂ compared to those of TiO₂ before lithiation.

SEM images of TiO₂ NT arrays both before and after lithiation are shown in Figure 2. Similar to our previous results, the amorphous (figure 2a) and anatase NT (figure 2c) grow vertically on the Ti foils with an outer diameter of ~70 nm. The length is around 400 nm depending on the reaction time.⁴¹ After calcination, the wall thickness increases slightly, leading to a smaller inner diameter for anatase TiO₂ compared with that of amorphous TiO₂. The morphologies of the samples after lithiation are also examined, as shown in Figure 2b and 2d. It is found that for both amorphous and anatase TiO₂, the morphologies remain intact after cycling. This observation is in good accord with results reported by Fang et al.¹³ It should be noted that the volume variation upon lithiation for TiO₂ is quite small (around 3%), and that a large surface to volume ratio and the presence of voids in nanotubes help accommodate the stress and strain. As a result, the lithiation process has little effect on the morphology of the aligned nanotubes.

The electrochemical performances of the TiO₂ NT specimens are further examined; the results are shown in Figure 3. The initial

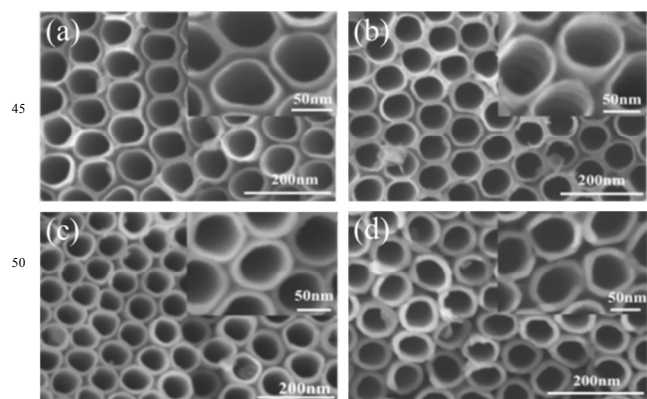


Figure 2. SEM images of (a) amorphous TiO₂ NT; (b) lithiated amorphous TiO₂ NT; (c) anatase TiO₂ NT; (d) lithiated anatase TiO₂ NT. (insets show magnified views of the TiO₂ NTs)

ial discharge and charge profiles for amorphous and anatase TiO₂ NT are presented in Figure 3a and 3b, respectively. From stage A to B, the NTs are discharged and insertion of lithium ions into TiO₂ occurs. In the charge process, the lithium ions are extracted from the TiO₂ framework and reach stage C. Obviously, amorphous and anatase TiO₂ NT exhibit different voltage plateaus. For anatase TiO₂, it presents a discharge and charge plateau at around 1.7 V and 1.9 V respectively, corresponding to the insertion and extraction of lithium ions. While for the as-made TiO₂, due to the large amount of defects and the disordered structure, it shows an expanded potential range. As a result, the curves show no obvious potential plateaus. The shape of the curves are in good agreement with the earlier reports on the amorphous and anatase TiO₂.^{12, 13, 48, 49} The amorphous TiO₂ NT delivers an initial discharge capacity of 311 mA h g⁻¹ and a charge capacity of 259 mA h g⁻¹ with a coulombic efficiency of 83%. The anatase TiO₂ NT delivers a first discharge and charge capacities of 201 and 180 mA h g⁻¹, respectively. The initial coulombic efficiency is 90%. It is conceivable that the defect rich and disordered structure in amorphous TiO₂ NT could supply more space for the insertion of lithium ions, leading to a higher capacity compared with that for anatase TiO₂. The cycling behaviors for TiO₂ NTs are shown in Figure 3c. It is concluded that both amorphous and anatase TiO₂ exhibit quite stable retention of capacity in the first 10 cycles after the initial decay of the capacity, which is due to the irreversible solid electrolyte

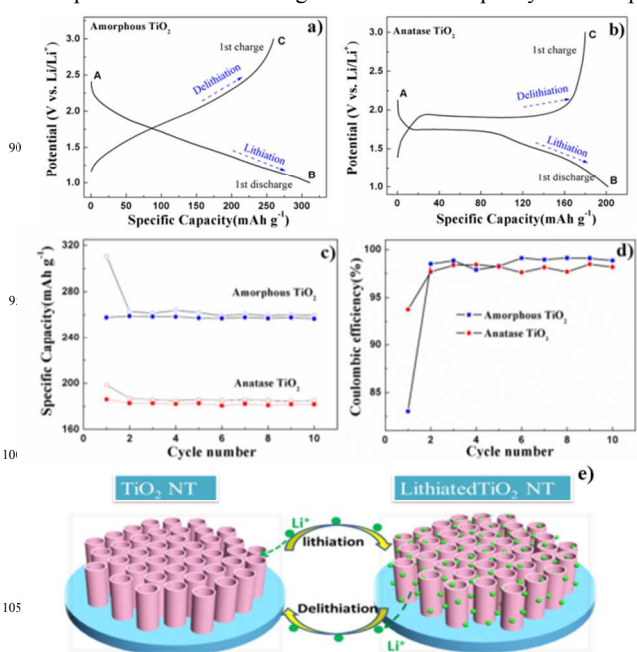


Figure 3. Initial charge-discharge profiles of (a) amorphous TiO₂ and (b) anatase TiO₂ at 100 mA g⁻¹ (A, B and C represent different stages for lithiation and delithiation); (c) Cycling behavior of amorphous and anatase TiO₂ in the first 10 cycles at 100 mA g⁻¹ in the voltage window of 1.0 to 3.0 V. (hollow dots: discharge curves; solid dots: charge curves) d) A comparison of Coulombic efficiency of amorphous TiO₂ and anatase TiO₂ in the first 10 cycles. e) Schematic representation of lithiation process in TiO₂ nanotube arrays.

ous TiO₂ NT may be due to the more trapped lithium ions inside the titanate framework at defect sites^{13, 50} and higher amount of solid electrolyte interface (SEI) layers forming in the thinner tube walls compared to that of anatase one. After 10 cycles, the discharge capacities for amorphous TiO₂ and anatase TiO₂ are stabilized at 260 mA h g⁻¹ and 185 mA h g⁻¹, respectively. As shown in Figure 3c and 3d, the cycle curves become flat and the coulombic efficiencies of both samples achieve around 97% starting from the second cycle, indicating superior cyclic performance. The stable cyclability for both NT should be ascribed to the intrinsic small volume variation and also the one dimensional nanotube morphology, which accommodate the stress and maintain the original structure very well. As demonstrated in figure 3e, upon cycling, lithium ions are reversibly intercalated and deintercalated into the self-organized TiO₂ nanotube arrays, where the structure and morphologies are essentially intact.

Ti L_{3,2}-edge and O K edge XANES: To characterize the electronic structure and local structure of the TiO₂ NT before and after lithiation, XANES at the Ti L_{3,2}-edge and the O K-edge have been obtained using partial, element specific X-ray fluorescence yield monitored with an energy-dispersive silicon drift detector (SDD), which generates a color-coded 2D display of excitation energy versus X-ray fluorescence energy.⁵¹ Figure S2 shows the 2D display of excitation energy across the Ti L_{3,2} and O K edge versus X-ray fluorescence energy recorded by a Silicon drift detector (SDD) with the relative intensity color bar as shown on the image. The Ti L_{3,2} and O K edge XANES spectra are obtained by monitoring the response of the corresponding fluorescence (dashed lines) as a function of excitation energy. There is clearly sufficient energy resolution separating the Ti L α (452.2 eV) and O K α (524.9 eV) fluorescence lines.

Figure 4 shows the Ti L_{3,2} edge XANES spectra for amorphous and anatase TiO₂ NT, henceforth denoted AM-TiO₂ and AN-TiO₂ respectively both before and after lithiation. The features of interest are marked by vertical dashed lines. Typical features arising from the transitions of Ti 2p electrons to previous unoccupied 3d electronic states in a distorted octahedral crystal field can be clearly identified. A weak shoulder doublet in all the compounds, denoted a and b, are related to transitions which are dipole forbidden, but is possible due to the multiple interaction.⁵² c and f are ascribed to the transition from 2p_{3/2} and 2p_{1/2} to t_{2g}, respectively while d, e and g are attributed to the transition from 2p_{1/2} to e_g.^{36, 41, 53, 54} It is interesting to note that relative intensity

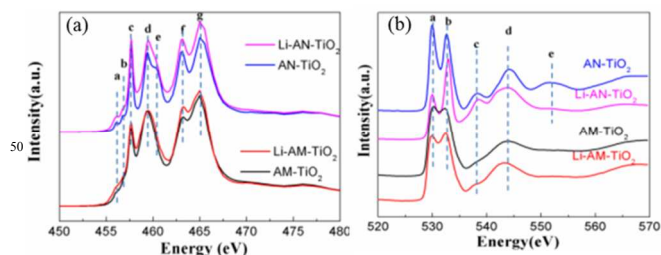


Figure 4. (a) Ti L_{3,2} edge XANES and (b) O K edge XANES of amorphous TiO₂ NT, anatase TiO₂ NT, lithiated amorphous and anatase TiO₂ NT obtained at stage B in figure 3. (AM-TiO₂: amorphous TiO₂; AN-TiO₂: anatase TiO₂)

of d and e is reversed in rutile TiO₂ and in SrTiO₃, where Ti is in a perfect octahedral environment there is no splitting and d and e merges into a single peak. It is apparent the d, e doublet in Fig. 4a is anatase like and more pronounced while it is blurred in amorphous TiO₂ NT. Since e_g states are sensitive to the variation in symmetry, the further splitting in spectra at e_g states of L₃ edge for anatase TiO₂ should be attributed to the distortion to D_{2d}.^{52, 54} Since as-made TiO₂ are amorphous and lack of long range ordering, the local distortion of Ti is an average of all arrangements, leading to the broadening of the e_g peak.

Turning to the spectra for lithiated samples, it is apparent that the spectra are quite similar to those before lithiation, indicating that the local environment and the electronic structure of Ti are well maintained after the introduction of lithium ions. Since the volume variation for TiO₂ is quite small and it is a tubal structure, the original local structures of the Ti-O framework are well kept after lithiation. Closer observation reveals a broadening feature at the e_g states (d and e) and also the pre-edges (a and b) for the lithiated anatase TiO₂ nanotube, which could be attributed to a slight amorphization or distortion of the crystalline TiO₂ framework by lithium ions as demonstrated from the XRD spectra where the (004) diffraction intensity is greatly reduced. It is conceivable that the lithium ions lied in the [001] direction of TiO₂ framework along the channels shown in Fig. 1 c). They are different from results reported from Okumura et al.,³² where they claimed a Ti⁴⁺ to Ti³⁺ transition upon lithiation at Ti L edge in sub-micro sized TiO₂-B phase. More importantly, they further compared it with the TiO₂-B nanowires of different size.⁵⁵ After lithiation, it is found that the Ti K-edge XAFS spectra of Li_xTiO₂-B nanowires remain unchanged, indicating that the local structural change for Ti is limited by nanoparticles without chemical states variation. Here, for TiO₂ nanotube arrays, no detectable shift of the absorption peaks at the Ti L_{3,2} edge is found, indicating that the lithium insertion does not lead to the local valence variation of Ti similar to nanowires reported by Okumura et al.,⁵⁵ instead, it may only change the interaction (e.g. covalence or ionicity) between Ti and O ions analogous to that reported by Zhou et al. previously.³⁶ Also, the slight increase in intensities of white line are evident for both lithiated amorphous and anatase TiO₂ at the L_{3,2} edge, indicating either electron depletion at Ti 3d projected orbital, or transition matrix elements effects due to the lithium intercalation or both.

Figure 4b probes the transitions of O 1s to unoccupied 2p states in the conduction band. The hybridization of Ti 3d and also 4s, 4p with O 2p determines the spectra features. The first two sharp peaks for a and b arise from hybridization with Ti 3d states while the following peaks are ascribed to the O 2p anti-bonding state and hybridization with s, p states of Ti.^{41, 53, 56} Crystalline anatase TiO₂ shows characteristic features similar to previously reported results,⁵⁷ while amorphous TiO₂ NT exhibit broadened and smoothed out features, for example, the loss of resonance e due to its low crystallinity and lack of long range order. However, the locally ordered features could still be tracked such as peaks a, b and e, similar to that in the Ti L_{3,2} edge XANES. The intensity ratio of peaks c to d at Ti L edge XANES of AM-TiO₂ is also lower compared with that of anatase, indicating a weaker crystal field or more under coordinated Ti atoms.⁵⁸

For the lithiated sample, we see that for the amorphous TiO₂, the

spectrum matched well with that of TiO_2 before lithiation indicating a well maintained local environment for O. The defects and disordered structure in amorphous TiO_2 may help supply extra space to accommodate lithium ions, resulting in little significant influence on the local chemistry for O atoms. However, closer examination indicate a slight increase for the peak intensity ratio of b to a and a slight energy shift of peak a toward lower energy upon lithiation. For the lithiated anatase TiO_2 , the peak intensity ratio of b to a increases significantly with a more pronounced feature at peak c and a smoothed out feature at e. A similar trend, albeit less noticeable, is also found in the amorphous TiO_2 group. Closer look reveals a noticeably weaker resonance at peak a for lithiated anatase TiO_2 . Peak a arises from the transition from O 1s to O 2p states which are hybridized with Ti t_{2g} states, while peak b refers to resonance to 2p states hybridized with Ti e_g states. We also examine the O K edge XANES of Li_2CO_3 , which is a common by-product during charging and discharging in carbonated based electrolyte, as shown in Figure S3. It exhibits a sharp edge jump at around

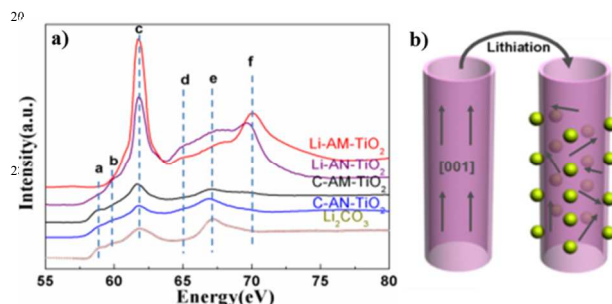


Figure 5. (a) Li K edge XANES for lithiated TiO_2 samples at stage B in figure 3 (denoted as Li-AM- TiO_2 and Li-AN- TiO_2), the samples after 10 discharge-charge cycles (denoted as C-AM- TiO_2 and C-AN- TiO_2) and standard Li_2CO_3 . (b) Schematic diagrams show process of the lithium driven random orientation for anatase TiO_2 NT. Yellow dot stands for lithium ions which arranges along [001].

539 eV which is assigned to the 1s electrons to the π^* (C = O) orbitals similar to that reported by Yang et al.⁵⁹ Further examination shows no resonances at a (530 eV) and b (532.6 eV) in the O K edge XANES of Li_2CO_3 ; thus the suppressed transition at peak a should be exclusively attribute to the lithiated TiO_2 , indicating increased occupied states on hybrid t_{2g} states and a charge transfer to 2p states of O character. Since lithium ions are trapped in the crystalline TiO_2 framework, the highly electropositive lithium ions may induce the charge relocation to the O 2p-Ti $3t_{2g}$ bands without affecting the local symmetry significantly. Okumura et al.⁵⁵ also found similar electron injection into the unoccupied O 2p orbital after lithiation for TiO_2 -B nanowires. Further, the enhanced transition at peak c indicate an increment corresponds to the anti-bonding O(2p) transition, which may be caused by the nearly linear O-Li-O arrangement where Li lies in the outgoing path of O photoelectrowave.^{36, 60} Finally, the smoothed out feature e may be due to the lack of long range ordering and slight amorphization, similar to the lack of splitting at e_g states observed at the Ti L_3 edge.

Li K edge XANES: Figure 5a shows the Li K edge XANES of

TiO_2 samples after initial lithiation and 10 cycles. The spectrum for Li_2CO_3 are also provided, which is a common component for solid electrolyte interphase in carbonate based electrolyte. Lithiated amorphous and anatase TiO_2 nanotubes show similar resonance. The intense transitions at 62 eV and 67.2 eV should be attributable to the multiple scattering of the p wave by the caging environment,⁵¹ while the edge jump at about 60 eV is highly suppressed in all samples, illustrating a more covalent feature for lithium ions and surrounded atoms. Similar to Li K edge XANES for LiCoO_2 as reported by Zhou et al.³⁶, where Li ions are also intercalated into the framework, the lithiated TiO_2 NT presents similar resonances with the main edge jump occurring at 62 eV. Upon further comparison of the XANES spectra, it is found that the Li_2CO_3 are formed after cycling. For Li-AN- TiO_2 , after initial lithiation process, the Li_2CO_3 is already formed as can be seen from the shoulder shown in peak e of the spectrum. Since one dimensional NT has a large surface to volume ratio, many sites are available for Li_2CO_3 to deposit and co-exist with lithiated TiO_2 . After 10 cycles of discharge and charge, Li ions are extracted from the TiO_2 framework, while the stable Li_2CO_3 left behind, thus C-AN- TiO_2 presents distinct resonance features originating from Li_2CO_3 , as shown in the first weak shoulder doublet (peak a and b) and also the edge jump at peak c and e. Similar trend could also be found in the amorphous TiO_2 group, where more significant features of Li_2CO_3 appeared after 10 cycles. Although it is still unclear what the resonance at 70 eV is, most probably arises from the lithiated TiO_2 , possibly a multiple scattering between Li and surrounded atoms in lithiated TiO_2 framework. Figure 5b shows schematic diagrams for anatase TiO_2 NT upon lithiation. During intercalation, lithium ions locate themselves along the [001] direction forming a nearly linear “O-Li-O” bond in the tubes, while the orientation for highly ordered anatase TiO_2 NT becomes distorted. Thus Li K edge XANES successfully tracks the intercalation of lithium into the TiO_2 framework and reveals the local structures for Li atoms.

Ti K edge XAFS: Ti K edge XAFS are also informative about the local structure around Ti atoms, as shown in Figure 6. The fluorescence yield (FLY) spectrum recorded on the amorphous TiO_2 sample (Figure S4) presents a spectrum feature similar to Ti (0) rather than TiO_2 . As we know, the penetration depth for X-rays at Ti K edge is around 20 μm based on calculation from X-ray calculator,⁶¹ since the TiO_2 arrays have a thickness of 400 nm, thus FLY spectrum could unveil the information coming from the Ti foil underneath. Surface sensitive total electron yield spectrum is thus used here for TiO_2 . Figure 6a shows the XANES spectrum of the pristine and lithiated TiO_2 samples. All the spectra present typical pre-edge features and the white line. For anatase TiO_2 , the pre-edge features are marked as a, b and c, which arise from hybridization of p, d orbitals of Ti atom and surrounded neighbors.⁶²⁻⁶⁵ Peak a is attributed to the quadruple transition of 1s to t_{2g} states of octahedral TiO_6 ,⁶⁶⁻⁶⁹ while peak b and c assignments are controversial - resonance b is either attributed to the 1s to e_g transition of octahedral TiO_6 or the transition to t_{2g} of neighboring octahedral.⁶⁷⁻⁶⁹ Peak c is attributed to the transition to e_g states of neighboring Ti atoms or 4p states of absorbing atoms.

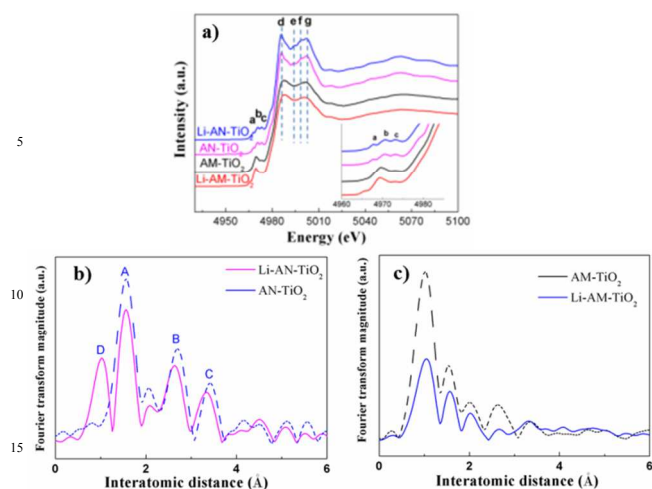


Figure 6. (a) XANES of Ti K edge and (b), (c) Fourier-transformed (FT) of the Ti K edge k^3 -weighted EXAFS spectra for amorphous and anatase TiO_2 , both before and after lithiation. (k-range for the FT: $2.6 - 12.8 \text{ \AA}^{-1}$) Inset of Figure 6(a) shows the magnified pre-edge region.

The weak shoulder between c and d stands for the $1s$ to $4p$ transition, while peak d is the higher lying p atomic orbitals.^{66, 70-73} It is further identified that anatase TiO_2 exhibits well-resolved peaks and sharp features at e and f due to its high crystallinity. In contrast, the amorphous TiO_2 is broader with blurred feature. The intense single pre-edge peak suggests Ti-oxide species exist in tetrahedral or pentahedral coordination.^{57, 74} For poor crystalline TiO_2 , a distorted or defective Ti environment is expected, leading to an increased distortion and thus increased resonance intensity at the pre-edge. Similar to Ti L edge XANES, the spectrum for lithiated samples is nearly the same as the pristine samples, indicating that the TiO_2 framework is well kept after lithiation due to the low volume variation and also the one dimensional tubal NT structure. The first derivative of XANES spectra shown in Figure S5 for lithiated TiO_2 nanotube is almost the same as the pristine ones without energy shift, further demonstrating that the chemical states is stable for Ti ions upon lithiation.

Fourier transformation (FT) of the EXAFS spectra⁷⁵ are shown in Figure 6b and 6c. The FTs for the two phases of TiO_2 exhibit distinct different characteristic features as shown in Figure S6. The coordination change can be clearly observed in the EXAFS region (in k space). For FT-EXAFS in Figure 6b, the A, B, C stands for the Ti-O, Ti-Ti and Ti-O-Ti coordination shells, respectively.^{76, 77} The existence of peak C indicates high crystallinity.⁷⁸ For amorphous TiO_2 , the Fourier transformation of EXAFS spectra is quite different, while the Ti-O, Ti-Ti and Ti-O-Ti bond could still be tracked as shown in Figure 6c. The one major intense peak at shorter interatomic distance centered at 1 \AA is too short even after a phase correction of $\sim 0.4 \text{ \AA}$ to be a real bond distance, it most likely arises from a combination of high k noise, the isolated Ti-oxide species of amorphous TiO_2 in tetrahedral or pentahedral coordination and the focusing effect of intervening Li in a chemically inhomogeneous Ti local environment. Turning to the spectra for the lithiated samples, we find that both of them exhibit similar EXAFS oscillations in the low k region compared to pristine samples but with noticeable

lower magnitudes and broadening, illustrating lower coordination number on average of Ti and hence an increase of disorder among them (larger static Debye-Waller factor). It should be noted that similar feature at position D (around 1 \AA in FT) for Li-AN- TiO_2 popped out after lithiation process, which is similar to that for the amorphous TiO_2 . The presence of Li can act as electron lens modifying the EXAFS with enhanced intensity in the FT. It is concluded that for anatase TiO_2 , the lithiation of the TiO_2 leads to at least partially amorphization of the pristine TiO_2 which are in agreement with the Ti L edge XANES.

Conclusions

The amorphous and anatase TiO_2 NT self-organized arrays have been successfully prepared and their lithium ion storage capabilities are examined. Both of the TiO_2 NTs exhibit stable cycling performances benefitting from the 1D nanostructure and also the inherent low volume variation. Amorphous TiO_2 NTs exhibit higher capacity than anatase TiO_2 NTs due to its higher intercalation sites for lithium ions from the disordered structure. A detailed XAFS analysis has been conducted on the pristine and lithiated TiO_2 at the Ti L, K and O K edge. XAFS reveals different local symmetry, distortion and crystallinity in amorphous and anatase TiO_2 . Li K edge XANES confirms the introduction of Li into TiO_2 framework, locating along the $[001]$ direction of TiO_2 framework and its presence induces charge relocation to the O $2p$ -Ti $3t_{2g}$ bands as demonstrated from the O K edge XANES. XANES and EXAFS spectra also reveal the slight lithiation induced amorphization of the TiO_2 , while the chemical states of Ti and O are well maintained. This work demonstrates a case study of the effects of lithiation process on structural variations for TiO_2 electrodes probed by the XAFS technique and could be easily extended to other electrodes and energy devices such as photovoltaic cells, capacitors and fuel cells.

Notes and references

^a Department of Mechanical and Materials Engineering, University of Western Ontario, London, Ontario, N6A 5B9 Canada. Tel: 15196612111 ext. 87759; E-mail: xsun@eng.uwo.ca

^b Department of Chemistry, University of Western Ontario, London, Ontario, N6A 5B7 Canada. Tel: 15196612111 ext. 86341; E-mail: tsham@uwo.ca

^c Soochow-Western Center for Synchrotron Radiation Research, Soochow University, and Institute of Functional Nano and Soft Materials, Soochow University, Suzhou, Jiangsu, 215123 China

^d Current address: Canadian Light Source Inc. 44 Innovation Boulevard, Saskatoon, Saskatchewan, S7N 2V3 Canada.

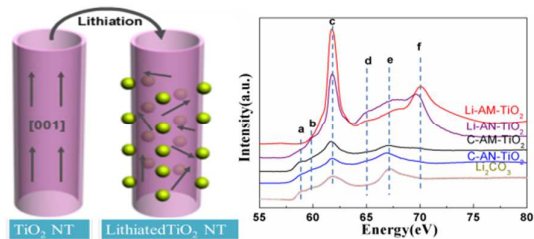
† Electronic Supplementary Information (ESI) available: EDS spectrum of amorphous TiO_2 nanotube, 2-D display of excitation energy across the Ti $L_{3,2}$ -edge and O K edge (y-axis) vs. fluorescence/scattered X-ray energy (x-axis) from Ti and O detected with a silicon drift detector, O K edge XANES of Li_2CO_3 powder, FLY spectrum of amorphous TiO_2 rooted on Ti foil and first derivative spectra of Ti K edge XAFS for amorphous and anatase TiO_2 , both before and after lithiation. See DOI: 10.1039/b000000x/

1. R. Asahi, T. Morikawa, T. Ohwaki, K. Aoki and Y. Taga, *Science*, 2001, 293, 269-271.
2. M. Law, L. E. Greene, J. C. Johnson, R. Saykally and P. D. Yang, *Nat Mater*, 2005, 4, 455-459.
3. B. Oregan and M. Gratzel, *Nature*, 1991, 353, 737-740.

4. T. Brousse, R. Marchand, P. L. Taberna and P. Simon, *J Power Sources*, 2006, 158, 571-577.
5. A. S. Arico, P. Bruce, B. Scrosati, J. M. Tarascon and W. Van Schalkwijk, *Nat Mater*, 2005, 4, 366-377.
6. A. R. Armstrong, G. Armstrong, J. Canales, R. Garcia and P. G. Bruce, *Adv Mater*, 2005, 17, 862-+.
7. L. Kavan, M. Kalbac, M. Zukalova, I. Exnar, V. Lorenzen, R. Nesper and M. Graetzel, *Chem Mater*, 2004, 16, 477-485.
8. S. Y. Huang, L. Kavan, I. Exnar and M. Graetzel, *J Electrochem Soc*, 1995, 142, L142-L144.
9. H. S. Zhou, D. L. Li, M. Hibino and I. Honma, *Angew Chem Int Edit*, 2005, 44, 797-802.
10. Q. Wang, Z. H. Wen and J. H. Li, *Adv Funct Mater*, 2006, 16, 2141-2146.
11. Y. S. Hu, L. Kienle, Y. G. Guo and J. Maier, *Adv Mater*, 2006, 18, 1421-+.
12. Y. G. Guo, Y. S. Hu, W. Sigle and J. Maier, *Adv Mater*, 2007, 19, 2087-+.
13. H. T. Fang, M. Liu, D. W. Wang, T. Sun, D. S. Guan, F. Li, J. G. Zhou, T. K. Sham and H. M. Cheng, *Nanotechnology*, 2009, 20.
14. H. Han, T. Song, E. K. Lee, A. Devadoss, Y. Jeon, J. Ha, Y. C. Chung, Y. M. Choi, Y. G. Jung and U. Paik, *Acs Nano*, 2012, 6, 8308-8315.
15. S. W. Kim, T. H. Han, J. Kim, H. Gwon, H. S. Moon, S. W. Kang, S. O. Kim and K. Kang, *Acs Nano*, 2009, 3, 1085-1090.
16. F. X. Wu, Z. X. Wang, X. H. Li and H. J. Guo, *J Mater Chem*, 2011, 21, 12675-12681.
17. J. M. Li, W. Wan, H. H. Zhou, J. J. Li and D. S. Xu, *Chem Commun*, 2011, 47, 3439-3441.
18. M. S. Whittingham and M. B. Dines, *J Electrochem Soc*, 1977, 124, 1387-1388.
19. M. Wagemaker, W. J. H. Borghols and F. M. Mulder, *J Am Chem Soc*, 2007, 129, 4323-4327.
20. M. Wagemaker, W. J. H. Borghols, E. R. H. van Eck, A. P. M. Kentgens, G. L. Kearley and F. M. Mulder, *Chem-Eur J*, 2007, 13, 2023-2028.
21. V. Luca, T. L. Hanley, N. K. Roberts and R. F. Howe, *Chem Mater*, 1999, 11, 2089-2102.
22. G. Sudant, E. Baudrin, D. Larcher and J. M. Tarascon, *J Mater Chem*, 2005, 15, 1263-1269.
23. U. Lafont, D. Carta, G. Mountjoy, A. V. Chadwick and E. M. Kelder, *J Phys Chem C*, 2010, 114, 1372-1378.
24. F. Bonino, L. Busani, M. Lazzari, M. Manstretta, B. Rivolta and B. Scrosati, *J Power Sources*, 1981, 6, 261-270.
25. H. Ade and H. Stoll, *Nat Mater*, 2009, 8, 281-290.
26. T. E. Westre, P. Kennepohl, J. G. DeWitt, B. Hedman, K. O. Hodgson and E. I. Solomon, *J Am Chem Soc*, 1997, 119, 6297-6314.
27. D. N. Wang, J. L. Yang, X. F. Li, J. J. Wang, R. Y. Li, M. Cai, T. K. Sham and X. L. Sun, *Cryst Growth Des*, 2012, 12, 397-402.
28. D. N. Wang, J. L. Yang, X. F. Li, D. S. Geng, R. Y. Li, M. Cai, T. K. Sham and X. L. Sun, *Energ Environ Sci*, 2013, 6, 2900-2906.
29. D. N. Wang, X. F. Li, J. L. Yang, J. J. Wang, D. S. Geng, R. Y. Li, M. Cai, T. K. Sham and X. L. Sun, *Phys Chem Chem Phys*, 2013, 15, 3535-3542.
30. T. Ohzuku, Z. Takehara and S. Yoshizawa, *Electrochim Acta*, 1979, 24, 219-222.
31. R. J. Cava, D. W. Murphy, S. Zahurak, A. Santoro and R. S. Roth, *J Solid State Chem*, 1984, 53, 64-75.
32. T. Okumura, T. Fukutsuka, A. Yanagihara, Y. Orikasa, H. Arai, Z. Ogumi and Y. Uchimoto, *Journal of Materials Chemistry*, 2011, 21, 15369-15377.
33. M. V. Koudriachova, *Chem Phys Lett*, 2008, 458, 108-112.
34. M. V. Koudriachova, *Phys Chem Chem Phys*, 2008, 10, 5094-5098.
35. B. J. Morgan and G. W. Watson, *J. Phys. Chem. Lett.*, 2011, 2, 1657-1661.
36. J. G. Zhou, H. T. Fang, J. M. Maley, M. W. Murphy, J. Y. P. Ko, J. N. Cutler, R. Sammynaiken, T. K. Sham, M. Liu and F. Li, *J Mater Chem*, 2009, 19, 6804-6809.
37. W. J. H. Borghols, D. Lutzenkirchen-Hecht, U. Haake, W. Chan, U. Lafont, E. M. Kelder, E. R. H. van Eck, A. P. M. Kentgens, F. M. Mulder and M. Wagemaker, *J Electrochem Soc*, 2010, 157, A582-A588.
38. W. Ra, M. Nakayama, W. Cho, M. Wakihara and Y. Uchimoto, *Phys Chem Chem Phys*, 2006, 8, 882-889.
39. G. Armstrong, A. R. Armstrong, P. G. Bruce, P. Reale and B. Scrosati, *Adv Mater*, 2006, 18, 2597-+.
40. D. H. Wang, D. W. Choi, J. Li, Z. G. Yang, Z. M. Nie, R. Kou, D. H. Hu, C. M. Wang, L. V. Saraf, J. G. Zhang, I. A. Aksay and J. Liu, *Acs Nano*, 2009, 3, 907-914.
41. L. J. Liu, J. Chan and T. K. Sham, *J Phys Chem C*, 2010, 114, 21353-21359.
42. T. Regier, J. Krochak, T. K. Sham, Y. F. Hu, J. Thompson and R. I. R. Blyth, *Nucl Instrum Meth A*, 2007, 582, 93-95.
43. T. Regier, J. Paulsen, G. Wright, I. Coulthard, K. Tan, T. K. Sham and R. I. R. Blyth, *Aip Conf Proc*, 2007, 879, 473-476.
44. Y. F. Hu, I. Coulthard, D. Chevrier, G. Wright, R. Igarashi, A. Sitnikov, B. W. Yates, E. L. Hallin, T. K. Sham and R. Reininger, *Sri 2009: The 10th International Conference on Synchrotron Radiation Instrumentation*, 2010, 1234, 343-346.
45. Y. F. Hu, L. Zuin, G. Wright, R. Igarashi, M. McKibben, T. Wilson, S. Y. Chen, T. Johnson, D. Maxwell, B. W. Yates, T. K. Sham and R. Reininger, *Rev. Sci. Instrum.*, 2007, 78.
46. S. Lee, I. J. Park, D. H. Kim, W. M. Seong, D. W. Kim, G. S. Han, J. Y. Kim, H. S. Jung and K. S. Hong, *Energ Environ Sci*, 2012, 5, 7989-7995.
47. H. T. Tung, J. M. Song, S. W. Feng, C. S. Kuo and I. G. Chen, *Phys Chem Chem Phys*, 2010, 12, 15133-15133.
48. Q. L. Wu, J. C. Li, R. D. Deshpande, N. Subramanian, S. E. Rankin, F. Q. Yang and Y. T. Cheng, *J Phys Chem C*, 2012, 116, 18669-18677.
49. I. Moriguchi, R. Hidaka, H. Yamada, T. Kudo, H. Murakami and N. Nakashima, *Adv Mater*, 2006, 18, 69-73.
50. Y. Y. Zhang, Y. X. Tang, S. Y. Yin, Z. Y. Zeng, H. Zhang, C. M. Li, Z. L. Dong, Z. Chen and X. D. Chen, *Nanoscale*, 2011, 3, 4074-4077.
51. S. L. Yang, D. N. Wang, G. X. Liang, Y. M. Yiu, J. J. Wang, L. J. Liu, X. L. Sun and T. K. Sham, *Energ Environ Sci*, 2012, 5, 7007-7016.
52. F. M. F. Degroot, M. O. Figueiredo, M. J. Basto, M. Abbate, H. Petersen and J. C. Fuggle, *Phys. Chem. Miner.*, 1992, 19, 140-147.
53. L. A. Grunes, R. D. Leapman, C. N. Wilker, R. Hoffmann and A. B. Kunz, *Phys Rev B*, 1982, 25, 7157-7173.

54. F. M. F. Degroot, J. C. Fuggle, B. T. Thole and G. A. Sawatzky, *Phys Rev B*, 1990, 41, 928-937.
55. T. Okumura, T. Fukutsuka, A. Yanagihara, Y. Orikasa, H. Arai, Z. Ogumi and Y. Uchimoto, *Chemistry of Materials*, 2011, 23, 3636-3644.
56. R. Brydson, H. Sauer, W. Engel, J. M. Thomas, E. Zeitler, N. Kosugi and H. Kuroda, *J Phys-Condens Mat*, 1989, 1, 797-812.
57. S. J. Stewart, M. Fernandez-Garcia, C. Belver, B. S. Mun and F. G. Requejo, *J. Phys. Chem. B* 2006, 110, 16482-16486.
58. G. S. Henderson, X. Liu and M. E. Fleet, *Phys. Chem. Miner.*, 2002, 29, 32-42.
59. R. M. Qiao, Y. D. Chuang, S. S. Yan and W. L. Yang, *Plos One*, 2012, 7.
60. M. V. Koudriachova, S. W. de Leeuw and N. M. Harrison, *Phys Rev B*, 2004, 69.
61. B. L. Henke, E. M. Gullikson and J. C. Davis, *At. Data Nucl. Data Tables* 1993, 55, 349-349.
62. F. Farges, G. E. Brown and J. J. Rehr, *Phys Rev B*, 1997, 56, 1809-1819.
63. V. Luca, S. Djajanti and R. F. Howe, *J. Phys. Chem. B* 1998, 102, 10650-10657.
64. L. X. Chen, T. Rajh, W. Jager, J. Nedeljkovic and M. C. Thurnauer, *Journal of synchrotron radiation*, 1999, 6, 445-447.
65. T. Rajh, J. M. Nedeljkovic, L. X. Chen, O. Poluektov and M. C. Thurnauer, *J. Phys. Chem. B* 1999, 103, 3515-3519.
66. Z. Y. Wu, G. Ouvrard, P. Gressier and C. R. Natoli, *Phys Rev B*, 1997, 55, 10382-10391.
67. T. Uozumi, K. Okada, A. Kotani, O. Durmeyer, J. P. Kappler, E. Beaurepaire and J. C. Parlebas, *Europhys. Lett.*, 1992, 18, 85-90.
68. M. A. Khan, A. Kotani and J. C. Parlebas, *J Phys-Condens Mat*, 1991, 3, 1763-1772.
69. K. Okada and A. Kotani, *J. Electron. Spectrosc. Relat. Phenom.*, 1993, 62, 131-140.
70. J. C. Parlebas, M. A. Khan, T. Uozumi, K. Okada and A. Kotani, *J. Electron. Spectrosc. Relat. Phenom.*, 1995, 71, 117-139.
71. L. Q. Wang, K. F. Ferris, A. N. Shultz, D. R. Baer and M. H. Engelhard, *Surf Sci*, 1997, 380, 352-364.
72. F. Farges, G. E. Brown and J. J. Rehr, *Geochim. Cosmochim. Acta* 1996, 60, 3023-3038.
73. Y. Joly, D. Cabaret, H. Renevier and C. R. Natoli, *Phys Rev Lett*, 1999, 82, 2398-2401.
74. L. X. Chen, T. Rajh, Z. Y. Wang and M. C. Thurnauer, *J. Phys. Chem. B* 1997, 101, 10688-10697.
75. G. Croft and M. J. Fuller, *Nature*, 1977, 269, 585-586.
76. Y. Kuwahara, T. Ohmichi, K. Mori, I. Katayama and H. Yamashita, *J Mater Sci*, 2008, 43, 2407-2410.
77. R. Bouchet, A. Weibel, P. Knauth, G. Mountjoy and A. V. Chadwick, *Chem Mater*, 2003, 15, 4996-5002.
78. K. Mori, H. Yamashita and M. Anpo, *Rsc Adv*, 2012, 2, 3165.

Table of Contents:



A detailed X-ray absorption fine structures study on amorphous and anatase TiO₂ nanotube arrays reveals the structural variation in titanate frame work and lithium arrangement during lithiation process.